Journal of Materials Chemistry A

Accepted Manuscript

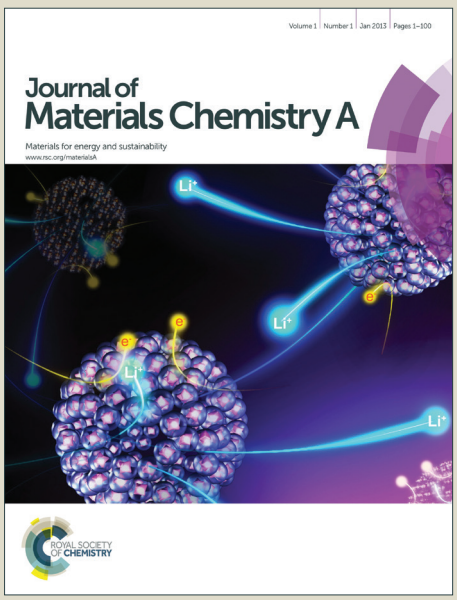

ROYAL SOCIETY OF CHEMISTRY

www.rsc.org/materialsA

Significantly improved photovoltaic performance of the triangular-spiral TPA(DPP-PN)$_3$ by appending planar phenanthrene units into the molecular terminals

Youming Zhang,[a] Xichang Bao,*[b] Manjun Xiao,[a,b] Hua Tan,*[a,c] Qiang Tao,[a] Yafei Wang,[a] Yu Liu,[a] Renqiang Yang*[b] and Weiguo Zhu*[a]

[a]*College of Chemistry, Xiangtan University, Key Lab of Environment-Friendly Chemistry and Application in Ministry of Education, Xiangtan 411105, China*

[b]*Qingdao Institute of Bioenergy and Bioprocess Technology, Chinese Academy of Sciences, Qingdao, Shandong 266101, China*

[c] *Institute of Polymer Optoelectronic Materials and Devices, State Key Laboratory of Luminescent Materials and Devices, South China University of Technology, Guangzhou 510640, China*

* Corresponding authors. Tel.: +86-731-58293377; fax: +86-731-58292251(W. Zhu).

Email addresses:

(W. Z.) zhuwg18@126.com,

(R. Y.) yangrq@qibebt.ac.cn,

(X. B.) baoxc@qibebt.ac.cn,

(H. T) tanhua815@126.com.

Abstract: A novel triangular-spiral conjugation molecule of TPA(DPP-PN)$_3$ using triphenylamine (TPA) as the donor core, diketopyrrolopyrrole (DPP) as acceptor arm and phenanthrene (PN) as the planar arene terminal, and it's counterpart of TPA-3DPP without the PN terminal were prepared. Their UV-vis absorption, electrochemistry and thermal stability, as well as hole mobility were preliminary investigated. Significantly red-shift UV-vis absorption profiles were observed for TPA(DPP-PN)$_3$ instead of TPA-3DPP in solution and solid state. The hole mobility of 1.67×10^{-4} $cm^2V^{-1}s^{-1}$ was obtained in the TPA(DPP-PN)$_3$/$PC_{71}BM$ blended film, which is 2.1 times higher than that of the TPA-3DPP/$PC_{71}BM$ blended film. Furthermore, the TPA(DPP-PN)$_3$/$PC_{71}BM$-based organic solar cells presented better photovoltaic property with the maximum power conversion efficiency of 3.67%, which is 1.9 times higher than that of TPA-3DPP/$PC_{71}BM$-based devices. The results confirm that appending planar PN terminals into TPA-3DPP with triangular-spiral shape is an efficient approach to improve photovoltaic performances for its resulting molecules.

KEYWORDS: Phenanthrene; Diketopyrrolopyrrole; Triphenylamine; Photovoltaic property; Organic solar cells

Introduction

Organic solar cells (OSCs) are considered to be a promising technology in the world's energy strategy due to their outstanding advantages such as low cost, easy fabrication, light weight, and compatibility with flexible substrates [1-5]. Over the past decades, most research efforts have focused on the solution-processed bulk hetero-junction (BHJ) polymer solar cells (PSCs) using a blend of p-type polymers and n-type soluble fullerene derivatives as the photoactive layer. The power conversion efficiency (PCE) over 9% was demonstrated in PSCs [6-10]. Recently, another branch of the OSCs, solution-processable small molecule organic solar cells (SM-OSCs) have gained considerable attentions because of their simple purification, defined molecular weight, and superior batch-to-batch reproducibility [6, 11-15]. The PCE over 8% was obtained in SM-OSCs, which is still lower than that in PSCs [8,16]. Therefore, it remains a great challenge for us to develop new high-performance solution-process-able small organic molecules and their SM-OSCs.

Among the developed small molecular donor materials, most of them are built by some electron donor (D) and electron acceptor (A) units, and have exhibited lower band-gap owing to an increasing double-bond character among the D and A units [17-20]. Furthermore, hybridization of the energy levels between the D and A units can drop off the highest occupied molecular orbit (HOMO) and the lowest unoccupied molecular orbit (LUMO) energy levels, which lead to an unusually small HOMO-LUMO energy separation [21]. Thus, the linear and star shape molecules with D-A

framework can highly act as light harvesting antennae and easily acquire enhanced photo- physical properties by tuning their molecular structures [22].

As we know, triarylamines (TPA) and/or diketopyrrolopyrrole (DPP) units have been widely used to construct D-A polymers and small molecules in OSCs because TPA has good electron-donating and hole-transporting abilities [23-31], DPP has strong light absorption and photochemical stability [32]. As a resulting, some low band-gap molecules with the DPP unit were presented and exhibited good photovoltaic performance in BHJ OSCs [33-39]. The successful examples were reported for polymers with a PCE of 8.0% [36] and for small molecules with a PCE of 5.79% [38] in the devices. In order to make full use of their advantages, both TPA and DPP units were recently employed to construct the low band-gap molecules due to the strong intramolecular D-A interaction. For example, Shi and Zhan reported some star-shaped D-A small molecules with a TPA core, three DPP arms and different substituted phenyl end-group [40-43]. The photovoltaic properties of these starburst molecules were observed to be improved by introducing different end-groups onto the DPP moiety. The maximum PCE of 2.13% was obtained in these OSCs without addition of DIO.

As planar arenes have a favorable end-to-end π-π interaction, which can improve the charge transport and interconnectivity [44-46]. some planar arenes, such as pyrene and phenanthrene were used as end group to construct linear-shape D-A small molecules. The planarity of these end-groups was demonstrated to highly affect device performances of their resulting small molecules. Considering that C2-phenanthrene has bigger conjugate degree than C2-naphthalene and substituted benzene (phenyl,

fluoro-phenyl and alkyl-phenyl), as well as can form smaller degree of planarity with other aromatic units than C9-anthracene, in the previous work, we developed a type of the linear-shape small molecules with π-stacking planar phenanthrene terminals [47]. As the star-shape small molecules have presented good solution processability, high absorption coefficient, excellent purity and dispersibility [17,18], in this paper, in order to further study the influence of the star framework and planar terminals on the photo-physical and photovoltaic properties, a new triangular-spiral small molecule of TPA-$(DPP\text{-}PN)_3$ was designed and synthesized (Scheme 1), where TPA, DPP and PN (phenanthrene) are used as donor core, acceptor arm and end group, respectively. As expected, the $TPA(DPP\text{-}PN)_3$ appending additional PN terminals exhibited broader and stronger absorption than the TPA-3DPP counterpart without the PN terminals. Furthermore, the $TPA(DPP\text{-}PN)_3$-based devices demonstrated better photovoltaic performance than the TPA-3DPP-based devices. The maximum PCE of 3.67% with a short circuit current density (J_{sc}) of 8.95 mA cm^{-2}, an open circuit voltage (V_{oc}) of 0.80 V, and a fill factor (*FF*) of 51% was obtained in the $TPA(DPP\text{-}PN)_3$ /$PC_{71}BM$ based devices under the illumination of AM 1.5 G, 100 mW cm^{-2}. The observed PCE, J_{sc}, and *FF* values are 1.9, 1.5 and 1.4 times higher than the corresponding values of the TPA-3DPP based cells. Compared to the reported star-shape small molecular analogues with different substituted phenyl end groups, this $TPA(DPP\text{-}PN)_3$ further displayed higher *FF* and PCE values in their OSCs [42]. This work confirms that the photovoltaic performance of the triangular-spiral molecules can be improved by appending additional planar phenanthrene terminals.

Results and Discussion

Synthesis

As shown in Scheme 2, 1,4,4,5,5-tetramethyl-2-(phenanthren-2-yl)-1,3,2-dioxaboro-lane (**PN-BPin**) and 2,5-bis(2-ethylhexyl)-3-(5-(phenanthren-2-yl)thiophen-2-yl)-6-(thiophen-2-yl)pyrrolo[3,4-c]pyrrole-1,4(2H,5H)-dione (**PN-DPP**) were synthesized by a common Suzuki coupling reaction using $PdCl_2$(dppf) or $Pd(PPh_3)_4$ as catalyst with a high yield over 80%. 3-(5-Bromothiophen-2-yl)-2,5-bis(2-ethylhexyl)-6-(5-(phenanthren-2-yl)-thiophen-2-yl)pyrrolo[3,4-c]pyrrole-1,4(2H,5H)-dione (**PN-DPP-Br**) was prepared by a direct substitution of PN-DPP with *N*-bromosuccinimide (NBS) in the solution of chloroform at dark room. Tris(4-(4,4,5,5-tetramethyl-1,3,2-dioxaborolan-2-yl)phenyl)amine (**TPA-3BPin**) was synthesized referred to the reported procedure [39]. The detailed synthesis and characterization of TPA(DPP-PN)$_3$ and TPA-3DPP are given in the experimental section. The molecular structures were characterized by ^{1}H NMR, MALDI-TOF mass spectra and element analysis, which confirm the well-defined chemical structures.

Thermal property

The thermal properties of the TPA(DPP-PN)$_3$ and TPA-3DPP were investigated by thermogravimetric analyses (TGA) under N_2 atmosphere at a heating rate of 10 ^{o}C min^{-1}. The TGA curves are shown in Figure 1 and the data are summarized in Table 1. Both of the small molecules exhibit a good thermal stability. The thermal decomposition temperatures (T_d) of 386 ^{o}C for TPA(DPP-PN)$_3$ and 409 ^{o}C for TPA-3DPP are

observed at the 5% weight-loss. It means that appending the planar PN terminals into TPA-3DPP has a decreasing effect on the thermal stability of the resulting molecules.

Electrochemical Properties

The electrochemical cyclic voltammetry (CV) curves of the TPA-3DPP and TPA-(DPP-PN)$_3$ films coated on a platinum electrode are shown in Figure 2. The empirical equations of E_{HOMO} = [-(E_{ox}-0.45)-4.8] and E_{LUMO} = [-(E_{red}-0.45)-4.8] eV are applied to estimate the HOMO and LUMO energy levels (E_{HOMO} and E_{LUMO}) by the onset of oxidation/reduction potentials (E_{ox}/E_{red}), where 0.45 V is a potential of ferrocene vs. Ag/AgCl and 4.8 eV is the energy level of Ag/AgCl to the vacuum energy level. The resulting electrochemical data are summarized in Table 1. The redox waves are observed with an obviously decreasing E_{ox} value from 0.86 to 0.62 V and a gradually increasing E_{red} value from -0.99 to -0.89 V for TPA(DPP-PN)$_3$ instead of TPA-3DPP. It implies that appending the planar PN terminals unit into TPA-3DPP can increase the reduction potential and decrease oxidation potential effectively. Compared to E_{HOMO}/E_{LUMO} values of -5.21/-3.66 eV for TPA-3DPP and -4.97/-3.46 eV for TPA-(DPP-PN)$_3$, a decreasing electrochemical band gap and an increasing HOMO energy levels are observed for TPA(DPP-PN)$_3$. It is noted that TPA(DPP-PN)$_3$ exhibits the lowest band gap of 1.51 eV among TPA-3DPP and its analogues with different substituted phenyl end groups [41,42]. Thus, we can speculate that TPA(DPP-PN)$_3$ is a potential candidate for electron donor material in OSCs.

Optical Properties

The UV-Vis absorption spectra of TPA(DPP-PN)$_3$ and TPA-3DPP in CH_2Cl_2 solution and neat films are presented in Figure 3a. The corresponding absorption data are listed in Table 2. In solution, both compounds exhibit similar UV spectra with two absorption bands, in which the high-lying band about 350 nm is assigned to the π - π* transitions of their conjugated backbones and another low-lying band about 600 nm originates from the intramolecular charge transfer (ICT) transitions from the TPA to the DPP units. In solid state, TPA(DPP-PN)$_3$ and TPA-3DPP show 30 ~ 40 nm red-shift absorption profiles in comparison to those in solution due to the enhanced intermolecular π - π stacking effect. Furthermore, the low-lying absorption peaks of TPA(DPP-PN)$_3$ have about 40 nm bathochromic shift compared to those of TPA-3DPP in solution and film, respectively. The maximum molar absorption coefficient (ε) value of 1.97×10^5 M^{-1} cm^{-1} is obtained for TPA(DPP-PN)$_3$, which is 1.35 times higher than that of TPA-3DPP**.** The increased absorption intensity of TPA(DPP-PN)$_3$ is due to the enlarged π-system and planar conformation of the PN terminals. In order to further understand the effect of the PN terminals on absorption, some star-shape analogues with the same TPA-3DPP framework and different terminals are listed in Table 2. A narrow optical band gap (E_g^{opt}) of 1.60 eV is presented for TPA(DPP-PN)$_3$, which is lower than those values (1.68 ~ 1.83 eV) for TAP-3DPP and some other star -shape analogues with the same TPA-3DPP framework and different terminals [42]. It indicates that TPA(DPP-PN)$_3$ has better absorption property and the lowest optical band gap [41,42]. Introducing the planar PN terminals into the star-shape TAP-3DPP is available to lower optical band gap for its resulting molecules. Figure 3b shows the

UV-vis absorption spectra of the blend films between TPA(DPP-PN)$_3$ (or TPA-3DPP) and PC$_{71}$BM in an optimized ratio of 1:2.5 (*w/w*). More intense absorption is observed in the TPA(DPP-PN)$_3$/PC$_{71}$BM blend film. Therefore, TPA(DPP-PN)$_3$ should exhibit better photovoltaic property that TPA-3DPP in OSCs.

Photovoltaic Performances

The photovoltaic performances of the TPA(DPP-PN)$_3$ and TPA-3DPP based OSCs were measured by the fabricating BHJ devices with a structure of ITO/PEDOT: PSS(30 nm)/ active layer (70 nm)/Ca(10 nm)/Al(100 nm). The active layer consists of TPA(DPP-PN)$_3$ (or TPA-3DPP) donor and PC$_{61}$BM (or PC$_{71}$BM) acceptor. In order to optimized the ratios between donor and acceptor, the TPA(DPP-PN)$_3$/PC$_{61}$BM based devices in various ratios from 1:1 to 1:3 (*w/w*) were fabricated. Figure S1 shows the resulting current density-voltage (*J-V*) characteristics of the TPA(DPP-PN)$_3$/PC$_{61}$BM based cells and the corresponding photovoltaic data are summarized in Table S1 (see supporting information) under AM 1.5 G illumination. The maximum PCE of 3.07% with V_{oc} of 0.81 V, J_{sc} of 8.12 mA/cm^2 and *FF* of 46.6% was obtained in the cells under an optimized ratio of 1:2.5 (*w/w*) between TPA(DPP-PN)$_3$ and PC$_{61}$BM. It is worth to note that PCE and *FF* values here for TPA(DPP-PN)$_3$/PC$_{61}$BM based cells are higher than the corresponding levels of its analogues/PC$_{61}$BM based cells [42]. It means that appending planar PN terminals is a better approach than appending substituted phenyl terminals in star-shape small molecules to improve photovoltaic performances for its resulting molecules. In order to further improve device performance, we took PC$_{71}$BM instead of PC$_{61}$BM as acceptor to fabricate new

BHJ-OSCs. The typical *J-V* characteristics are shown in Figure 4 under illumination of AM 1.5 G, 100 mW cm^{-2} and the corresponding device parameters are summarized in Table 3. It is found that the TPA(DPP-PN)$_3$/PC_{71}BM based device presented the best photovoltaic performance With increasing PCE, J_{sc} and *FF* levels. The maximum PCE of 3.67% with V_{oc} of 0.80 V, J_{sc} of 8.95 mA cm^{-2} and *FF* of 51% is obtained. To our knowledge, the PCE value here is the highest level among the reported star-shaped small molecules with TPA-DPP or TPA-3DPP framework in the single BHJ OSCs [40-42]. In contrast, the TPA-3DPP/ PC_{71}BM-based device displayed a lower PCE of 1.91% with V_{oc} of 0.91 V, J_{sc} of 5.85 mA cm^{-2} and *FF* of 36%. The significant increased PCE and J_{sc} for the TPA(DPP-PN)$_3$/PC_{71}BM-based devices should be related to the enhanced absorption intensity of TPA(DPP-PN)$_3$.

In order to further explain why TPA(DPP-PN)$_3$-based devices exhibited better photovoltaic property, the surface morphology for the blend films, as well as the external quantum efficiency (*EQE*) and charge transport property for the devices were measured. Fig. S2 shows the tapping-mode AFM images of the TPA-3DPP/PC_{71}BM and TPA(DPP-PN)$_3$/PC_{71}BM blend films on glass/ITO/PEDOT:PSS substrate recorded by atomic force microscopy (AFM) (See supporting information). The surface roughnesses of 0.290 nm for TPA(DPP-PN)$_3$ and 0.345 nm for TPA-3DPP are observed in their blend films. It implies that the TPA(DPP-PN)$_3$/PC_{71}BM blend film has better surface morphology, which is in favour of increasing PCE and J_{sc} values. The isolated spherical domains with approximate sizes of 24-120 and 24-80 nm are estimated in the TPA-3DPP/ and TPA(DPP-PN)$_3$/PC_{71}BM blend films, respectively.

These large strip domains for the TPA-3DPP/$PC_{71}BM$ blend film maybe due to the molecular aggregation of TPA-3DPP in solid state.

Figure 5 shows the *EQE* curves of the TPA$(DPP\text{-}PN)_3$/$PC_{71}BM$ and TPA-3DPP/ $PC_{71}BM$ based devices. Although both devices exhibit almost identically spectral response ranges from 300 nm to 700 nm, but markedly different *EQE* values are observed. The maximum *EQE* of 51% at 600 nm for the TPA$(DPP\text{-}PN)_3$/$PC_{71}BM$ based device is much higher than that (36% at 470 nm) for the TPA-3DPP/$PC_{71}BM$ based device. This increased *EQE* value for the TPA$(DPP\text{-}PN)_3$/$PC_{71}BM$ device is attributed to the increased absorption intensity by appending π-stacking planar PN terminals in TPA$(DPP\text{-}PN)_3$, which can make the photoactive layer adsorb more pho-tons to improve J_{sc}. Based on the J_{sc} value of 9.05 mA cm^{-2} integrated from the *EQE*, it is found that the calculated J_{sc} value is consistent with experimental value of the TPA$(DPP\text{-}PN)_3$ based devices.

Figure 6 shows the *J-V* characteristics of the hole-only devices with a structure of ITO/ PEDOT: PSS (30 nm)/active layer (180 or 220 nm)/ MoO_3 (5 nm)/Ag (80 nm). Here, the active layer consists of TPA$(DPP\text{-}PN)_3$ (or TPA-3DPP) and $PC_{71}BM$. The hole mobilities of devices are calculated via space-charge-limited-current (SCLC) model. The hole mobility of 1.67×10^{-4} and 7.92×10^{-5} cm^2 V^{-1} s^{-1} are observed in the TPA$(DPP\text{-}PN)_3$ and TPA-3DPP based devices, respectively. Obviously, the hole mobi -lity of the TPA$(DPP\text{-}PN)_3$/$PC_{71}BM$ based device is 2.1 times higher than that of the TPA-3DPP/$PC_{71}BM$ based device. The increasing hole mobility is responsible for the improved *FF* value in the optimized TPA$(DPP\text{-}PN)_3$/$PC_{71}BM$ device. Therefore,

appending the planar PN units into the star-sharp molecular terminals can promote photovoltaic property for its molecules in organic solar cells.

Conclusions

In summary, a novel triangular-spiral small molecule of TPA(DPP-PN)$_3$ was prepared with additional PN end-capped units on the basis of the TPA-3DPP counterpart. Its photovoltaic performance and hole mobility of the TPA(DPP-PN)$_3$-based devices are significantly improved owing to appending the π-stacking planar PN terminals into the TPA-3DPP parent. The optimized TPA(DPP-PN)$_3$/$PC_{71}BM$-based device presented a dramatically enhanced PCE of 3.67% with a J_{sc} of 8.95 mA cm^{-2} and *FF* of 51%, which is highest among the star-shape molecules with the same TPA -3DPP framework and different appending terminals. The results indicate that the structural modifications by appending planar PN terminals in the star-shaped TPA-3DPP parent could significantly enhance the device performances for its resulting molecules.

Experimental Section

*4,4,5,5-tetramethyl-2-(phenanthren-2-yl)-1,3,2-dioxaborolane (**PN-BPin**).*

To 20 mL of dry 1,4-dioxane were added 2-bromophenanthrene (257 mg, 1 mmol), bis(pinacolato)diboron (305 mg, 1.2 mmol), potassium acetate (525 mg, 5 mmol) and [1,10-bis -(diphenylphosphino)-ferrocene] dichloroplladium (22 mg, 0.03 mmol). The mixture was degassed for 30 mim with nitrogen flow and heated to reflux for 24 h under the protection of nitrogen. After cooled to room temperature, the mixture was extracted with DCM (3 × 20 mL) and the combined organic layer was dried over

anhydrous magnesium sulfate. The solvent was removed off by rotary evaporation and the residue was passed through a flash silica gel column using PE-DCM (*V/V*, 4:1) as the eluent to give white solid of PN-BPin (271 mg, yield 89.1%). ^{1}H NMR (400 MHz, $CDCl_3$), δ (ppm): 8.70 (dd, J = 8.0 Hz, 2H), 8.39 (s, 1H), 8.04 (d, J = 8.0 Hz, 1H), 7.89 (d, J = 7.4 Hz, 1H), 7.72-7.79 (m, 2H), 7.61-7.66 (m, 2H), 1.26 (s, 12H). GC-MS Calcd for $C_{20}H_{21}BO_2$ $[M]^+$, 304.1; Found, 304.1.

*2,5-bis(2-ethylhexyl)-3-(5-(phenanthren-2-yl)thiophen-2-yl)-6-(thiophen-2-yl) pyrrolo[3,4-c]pyrrole-1,4(2H,5H)-dione (**PN-DPP**).*

To a mixture of PN-BPin (170 mg, 0.56 mmol), 3-(5-bromo-thiophen-2-yl)-2,5-bis(2-ethylhexyl)- 6-(thiophen-2-yl)pyrrolo[3,4-c]pyrrole-1,4(2*H*,5*H*)-dione (DPP-Br, 280 mg, 0.47 mmol) and tetrakis-(triphenylphosphine) palladium ($Pd(PPh_3)_4$, 16 mg) was added a degassed mixture of toluene (15 mL), anhydrous ethanol (8 mL) and 2 M potassium carbonate aqueous solution (1 mL). The mixture was refluxed for 24 h under the protection of nitrogen. After cooled to room temperature, the mixture was poured into water (200 mL). It was extracted with DCM (3×20 mL) and the combined organic layer was dried over anhydrous magnesium sulfate. The solvent was removed off by rotary evaporation and the residue was passed through a flash silica gel column with PE-DCM (*V/V*, 3:1) as the eluent to give an red solid (263 mg, yield 80.0%). ^{1}H NMR ($CDCl_3$, 400 MHz), δ (ppm): 9.02 (s, 1H), 8.91 (s, 1H), 8.67-8.73 (m, 2H), 8.17 (s, 1H), 7.95 (d, J = 8.4Hz, 1H), 7.90 (d, J = 7.4Hz, 1H), 7.79 (s, 2H), 7.67-7.69 (m, 2H), 7.64 (s, 2H), 7.26 (s, 1H), 4.06 (d, J = 22.4 Hz, 4H), 1.88-1.98 (m, 2H), 1.25-1.39 (m, 16H), 0.89-0.95 (m, 12H). MALDI-MS Calcd for $C_{44}H_{48}N_2O_2S_2$ $[M]^+$,

700.316; Found, 700.377. ^{13}C NMR (100 MHz, $CDCl_3$), δ (ppm): 10.6, 14.1, 23.1, 23.7, 28.5, 30.3, 39.2, 45.9, 108.0, 108.1, 111.9, 122.7, 123.6, 124.3, 124.7, 125.5, 126.7, 126.9, 127.9, 128.3, 128.6, 129.9, 130.3, 130.4, 132.3, 132.2, 132.3, 135.1, 136.9, 140.2, 149.5, 161.6, 161.8.

3-(5-bromothiophen-2-yl)-2,5-bis(2-ethylhexyl)-6-(5-(phenanthren-2-yl)thioph-en-2-yl)pyrrolo[3,4-c]pyrrole-1,4(2H,5H)-dione (***PN-DPP-Br***).

PN-DPP (225 mg, 0.321 mmol) and *N*-bromosuccinimide (57 mg, 0.321 mmol) were dissolved into chloroform (20 mL) in a two-neck round flask under argon protection. The mixture was protected from light and stirred at room temperature for 2 h. The solvent was removed off by rotary evaporation and the residue was passed through a flash silica gel column with PE-DCM (*V/V*, 4:1) as the eluent to give a red solid (210 mg, yield 84.2%). ^{1}H NMR ($CDCl_3$, 400 MHz), δ (ppm): 9.03 (d, J = 3.8 Hz, 1H), 8.66-8.72 (m, 2H), 8.63 (d, J = 4.0 Hz, 1H), 8.16 (s, 1H), 7.89-7.93 (m, 2H), 7.78 (d, J = 2.8 Hz, 2H), 7.69-7.73 (m, 1H), 7.64 (d, J = 4.0 Hz, 2H), 7.22 (d, J = 4.0 Hz, 1H), 4.10 (d, J = 6.8 Hz, 2H), 3.96 (d, J = 8Hz, 2H), 1.95-1.97 (m, 1H), 1.92-1.94 (m, 1H), 1.26-1.39 (m, 16H), 0.88-0.95 (m, 12H). MALDI-MS Calcd for $C_{44}H_{47}BrN_2O_2S_2$ $[M]^+$, 778.226; Found, 780.246. ^{13}C NMR (100 MHz, $CDCl_3$), δ (ppm): 10.5, 14.0, 23.1, 23.7, 28.4, 30.2, 39.2, 46.1, 107.8, 108.3, 118.4, 122.7, 123.6, 124.2, 124.7, 125.4, 126.7, 127.0, 128.0, 129.9, 130.5, 131.0, 132.2, 132.3, 134.9, 137.3, 149.9.

*tris(4-(4,4,5,5-tetramethyl-1,3,2-dioxaborolan-2-yl)phenyl)amine (**TPA-3Bpin**)*

To 50 mL of dry 1,4-dioxane were added tris(4-bromophenyl)amine (734 mg, 1.54

mmol), bis(pinacolato)diboron (1.56 g, 6.14 mmol), potassium acetate (4.8 g, 46 mmol) and [1,10-bis(diphenylphosphino)-ferrocene] dichloroplladium (101 mg). The mixture was heated to reflux for 24 h under the protection of nitrogen. After cooled to room temperature, the mixture was extracted with DCM (3 × 20 mL) and the combined organic layer was dried over anhydrous magnesium sulfate. The solvent was removed by rotary evaporation and the residue was passed through a flash silica gel column using PE-DCM (*V/V*, 3:1) as the eluent to give white solid (614 mg, yield 64%). ^{1}H NMR (400 MHz, $CDCl_3$), δ (ppm): 7.68 (d, J = 8.2 Hz, 6H), 6.97 (d, J = 8.6 Hz, 6H),1.34 (s, 36H). MALDI-MS Calcd for $C_{36}H_{49}B_3NO_6$ $[M]^+$, 623.376; Found, 623.431.

*tris(4(2,5-bis(2-ethylhexyl)-3-thiophen-2-yl)-6-(thiophen-2-yl)-pyrrolo[3,4-c]pyrrole-1,4(2H,5H)-dione)amine (**TPA-3DPP**)*

To a mixture of *DPP-Br* (148 mg, 0.245 mmol), *TPA-3Bpin* (44 mg, 0.07 mmol), and tetrakis(triphenylphosphine) palladium [$Pd(PPh_3)_4$] (8 mg) was added a degassed mixture of toluene (20 mL), anhydrous ethanol (5 mL) and 2 M potassium carbonate aqueous solution (1 mL). The mixture was refluxed for 6 h under the protection of nitrogen. After cooled to room temperature, the mixture was poured into water (80 mL). It was extracted with DCM (3 × 30 mL) and the combined organic layer was dried over anhydrous magnesium sulfate. The solvent was removed by rotary evaporation and the residue was passed through a flash silica gel column with PE-DCM (*V/V*, 1:2) as the eluent to give red solid (106 mg, yield 83.5%). ^{1}H NMR ($CDCl_3$, 400 MHz), δ (ppm): 8.99 (d, J = 4.0Hz, 3H), 8.88 (m, 3H), 7.43 (d, J = 8.2

Hz, 9H), 7.28 (m, 3H), 7.21(d, *J* = 8.4 Hz, 6H), 4.04 (d, *J* = 12.0 Hz, 12H), 1.27 (m, 48H), 1.90 (m, 6H), 0.88 (m, 36H). MALDI-MS Calcd for $C_{108}H_{129}N_7O_6S_6$ $[M]^+$, 1811.833; Found, 1812.969. Anal. Calcd for $C_{108}H_{129}N_7O_6S_6$: C, 71.52; H, 7.17; N, 5.41; S, 10.61. Found: C, 70.98; H, 7.91; N, 5.06; S, 10.29.

*tris(4(2,5-bis(2-ethylhexyl)-3-(5-(phenanthren-2-yl)thiophen-2-yl)-6-(thiophen -2-yl)-pyrrolo[3,4-c]pyrrole-1,4(2H,5H)-dione)amine (**TPA(DPP-PN)$_3$**)*

To a mixture of *P-DPP-Br* (273 mg, 0.35 mmol), *TPA-3Bpin* (62 mg, 0.1 mmol), and tetrakis(triphenylphos-phine) palladium [$Pd(PPh_3)_4$] (11 mg) was added a degassed mixture of toluene (30 mL), anhydrous ethanol (10 mL) and 2 M potassium carbonate aqueous solution (1 mL). The mixture was refluxed for 24 h under the protection of nitrogen. After cooled to room temperature, the mixture was poured into water (80 mL). It was extracted with DCM (3 × 30 mL) and the combined organic layer was dried over anhydrous magnesium sulfate. The solvent was removed by rotary evapo-ration and the residue was passed through a flash silica gel column with PE-DCM (*V/V*, 1:4) as the eluent to give red solid (98 mg, yield 42%). ^{1}H NMR ($CDCl_3$, 400 MHz), δ (ppm): 9.03(d, *J* = 3.6 Hz, 6H), 8.57 (d, *J* = 7.6 Hz, 6H), 8.05 (s, 3H), 7.83(d, *J* = 5.6Hz, 6H), 7.69 (m, 6H), 7.62 (m, 3H), 7.58 (d, *J* = 8.4 Hz, 12H), 7.40 (d, *J* = 3.4Hz, 3H), 7.14 (d, *J* = 8.2 Hz, 6H), 4.07 (d, *J* = 7.8 Hz, 12H), 1.96 (m, 6H), 1.36 (m, 48H), 0.92 (m, 36H). MALDI-MS Calcd for $C_{150}H_{153}N_7O_6S_6$ $[M]^+$, 2340.021; Found, 2340.987. Anal. Calcd for $C_{150}H_{153}N_7O_6S_6$: C, 76.92; H, 6.58; N, 4.19; S, 8.21. Found: C, 75.95; H, 6.42; N, 3.94; S, 7.81.

Acknowledgements

The major program for cultivation of the National Natural Science Foundation of China (91233112), the National Natural Science Foundation of China (21172187, 51273168, 20102139 and 61107090), the Key Project of Hunan Province Education Department (13A102), the Innovation Group and Xiangtan Joint Project of Hunan Natural Science Foundation (12JJ7002 and 12JJ8001), the Scientific Research Fund of Hunan Provincial Education Department (11CY023, 12B123), the Scientific Research Fund of Xiangtan University (11QDZ18, 2011XZX08), the Open Fund of the State Key Laboratory of Luminescent Materials and Devices (South China University of Technology, 2014-skllmd-10) and the Postgraduate Science Foundation for Innovation in Hunan Province (CX2013B268).

References

[1] Y.J. Cheng, S.H. Yang, C.S. Hsu, *Chem. Rev.* 2009**, 109**, 5868.

[2] Y. Lin, Y.F. Li, X.W. Zhan, *Chem. Soc. Rev.* 2012, **41,** 4245.

[3] K. Walzer, B. Maennig, M. Pfeiffer, K. Leo, *Chem. Rev.* 2007, **107**, 1233.

[4] S. Günes, H. Neugebauer, N. S. Sariciftci, *Chem. Rev.* 2007, **107**, 1324.

[5] Y.S. Chen, X.J, Wan, G.K. Long, *Acc. Chem. Res.* 2013, **46**, 2645.

[6] B. Walker, C. Kim, T.Q. Nguyen, *Chem. Mater.* 2011, **23**, 470.

[7] S.O. Kim, Y. S, Kim, H.J. Yun, I. Kang, Y.W. Yoon, N. Shin, H.J. Son, H.G. Kim, M.J. Ko, B.S. Kim, S.K. Kwon, *Macromolecules* 2013**, 46**, 3861.

[8] Z.C. He, C.M Zhong, S.J. Su, M. Xu, H.B. Wu, Y. Cao, *Nat. Photon*. 2012, **6**, 593.

[9] M.J. Zhang, Y. Gu, X. Guo, F. Liu, S.Q. Zhang, L.J. Huo, T.P. Russell, J.H. Hou, *Adv. Mater*. 2013, **35**, 4944.

[10] Xi. Guo, S.R. Puniredd, M. Baumgarten, W. Pisula, K. Müllen, *Adv. Mater.* **2013**, **25**, 5467.

[11] B. Walker, A.B. Tamayo, X.D. Dang, P. Zalar, J.H. Seo, A. Garcia, M. Tantiwiwat, T.Q. Nguyen, *Adv. Funct. Mater.* 2009**, 19**, 3063.

[12] J.A. Mikroyannidis, S.S. Sharma, Y.K. Vijay, G.D. Sharma, *ACS Appl. Mater. Interfaces.* 2009, **2**, 270.

[13] S. Loser, C.J. Bruns, H. Miyauchi, R.P. Ortiz, A. Facchetti, S.I. Stupp, T.J. Marks, *J. Am. Chem. Soc.* 2011, **133**, 8142.

[14] G. Pozzi, S. Orlandi, M. Cavazzini, D. Minudri, L.A Macor, L. Otero, F. Fungo, *Org. Lett.* 2013, **15**, 4642.

[15] J. Zhang, G.L. Wu, C. He, D. Deng, Y.F. Li, *J. Mater. Chem*. 2011, **21***,* 3768.

[16] J.Y. Zhou, Y. Zuo, X.J. Wan, G.K. Long, Q. Zhang, W. Ni, Y.S. Liu, Z. Li, G.R. He, C.X. Li, B. Kan, M.M Li, Y.S. Chen, *J. Am. Chem. Soc.* 2013, **135***,* 8484.

[17] O. Alévêque, P. Leriche, N. Cocherel, P. Frère, A. Cravino, J. Roncali, *Sol. Energy Mater. Sol. Cells.* 2008, **92**, 1170.

[18] L. Ji, Q. Fang, M.S. Yuan, Z.Q. Liu, Y.X. Shen, H.F. Chen, *Org. Lett.* 2010**, 12***,* 5192.

[19] Y. Nicolas, P. Blanchard, E. Levillain, M. Allain, N. Mercier, J. Roncali, *Org. Lett.* 2004, **6**, 273.

[20] T. Kashiki, M. Kohara, I. Osaka, E. Miyazaki, K. Takimiya, *J. Org. Chem*. 2011,

76, 4061.

[21] G. Qian, Z.Y. Wang, *Chem. Asian J.* 2010, **5**, 1006.

[22] Y.W. Li, Q. Guo, Z.F. Li, J.N. Pei, W.J. Tian, *Energy Environ. Sci.* 2010**, 3**, 1427.

[23] J. Zhang, Y. Yang, C. He, D. Deng, Z.B. Li, Y.F. Li, *J. Phys. D: Appl. Phys.* 2011, **44**, 475101.

[24] P. Dutta, W. Yang, S.H. Eom, S.H. Lee, *Org. Electron.* 2012, **13**, 273.

[25] S.L, Zhang, X. Wang, A.L. Tang, J.H. Huang, C.L. Zhan J.N. Yao, *Phys. Chem. Chem. Phys***.**, 2014,**16**, 4664.

[26] Q. Liu, H.M. Zhan, C.L. Ho, F.R. Dai, Y.Y. Fu, Z.Y. Xie, L.X. Wang, J.H. Li, F. Yan, S.P. Huang, W.W. Wong, *Chem. Asian J.* 2013, **8**, 1892.

[27] H.X. Shang, H.J. Fan, Y. Liu, W.P. Hu, Y.F. Li, X.W. Zhan, *Adv. Mater.* 201**1,** **23**, 1554.

[28] K. Do, C. Kim, K. Song, S.J. Yun, J.K. Lee, J. Ko, *Sol. Energy Mater. Sol. Cells* 2013**, 115**, 52.

[29] J. Zhang, D. Deng, C. He, Y.J. He, M.J. Zhang, Z.G. Zhang, Z.J. Zhang, Y.F. Li, *Chem. Mater.* 2011**, 23**, 817.

[30] J. Zhang, Y. Yang, C. He, Y.J. He, G.J. Zhao, Y.F. Li, *Macromolecules* 2009**, 42***,* 7619.

[31] Y.Z. Lin, Z.G. Zhang, H.T. Bai, Y.F. Li, X.W. Zhan, *Chem. Commun*. 2012, **48**, 9655.

[32] C. B. Nielsen, M. Turbiez, I. McCulloch, *Adv. Mater*. 201**3, 2***5*, 1859.

[33] H. Tan, X.P. Deng, J.T Yu, B.F. Zhao, Y.F. Wang, Y. Liu, W.G. Zhu, H.B. Wu, Y. Cao, *Macromolecules* 2013**, 4***6*, 113.

[34] I. Meager, R.S. Ashraf, S. Mollinger, B.C. Schroeder, H. Bronstein, D. Beatrup, M.S. Vezie, T. Kirchartz, A. Salleo, J. Nelson, I. McCulloch, *J. Am. Chem. Soc.* 2013**, 135**, 11537.

[35] K.H. Hendriks, G.H.L. Heintges, V.S. Gevaerts, M.M. Wienk, R.A.J. Janssen, *Angew. Chem. Int. Ed.* 2013**, 52***,* 1.

[36] S. Albert-Seifried, D.H. Ko, Sven Hüttner, C. Kanimozhi, S. Patil, R.H. Friend, *Phys. Chem. Chem. Phys.*, 201**4**,**16**, 6743.

[37] Y.Z. Lin, L.C Ma, Y.F. Li, Y.Q. Liu, D.B. Zhu, X.W. Zhan, *Adv. Energy Mater.* 2013**, 3**, 1166.

[38] J.H. Huang, C.L. Zhan, X. Zhang, Y. Zhao, Z.H. Lu, H. Jia, B. Jiang, J. Ye, S.L. Zhang, A.L. Tang, Y.Q. Liu, Q.B. Pei, J.N. Yao, *ACS Appl. Mater. Interfaces.* 2013**, 5**, 2033.

[39] Y.Z. Lin, P. Cheng, Y.F. Li, X.W. Zhan, *Chem. Commun,* 2012, **48**, 4773.

[40] D. Sahu, C.H. Tsai, H.Y. Wei, K.C. Ho, F.C. Chang, C.W. Chu, *J. Mater. Chem.* 2012, **22**, 7945.

[41] A.L. Tang, L.J. Li, Z.H. Lu, J.H. Huang, H. Jia, C.L. Zhan, Z.A. Tan, Y.F. Li, J.N. Yao, *J. Mater. Chem. A,* 2013, **1**, 5747.

[42] J.Y. Pan, L.J. Zuo, X.L. Hu, W.F. Fu, M.R. Chen, L.Fu, X. Gu, H.Q. Shi, M.M. Shi, H.Y. Li, H.Z. Chen, *ACS Appl. Mater. Interfaces.* 2013**, 5**, 972.

[43] Y.Z. Lin, H.F. Dam, T.R. Andersen, E. Bundgaard, W.F. Fu, H.Z. Chen, F.C.

Krebs, X.W. Zhan, *J. Mater. Chem. C,* 2013**, 1**, 8007.

[44] O.P. Lee, A.T. Yiu, P.M. Beaujuge, C.H. Woo, T.W. Holcombe, J.E. Millstone, J.D. Douglas, M.S. Chen, J.M.J. Fréchet, *Adv. Mater.* 2011**, 23**, 5359.

[45] Z.L. Wu, A.Y. Li, B.H. Fan, F. X, C. Adachi, J. O, *Sol. Energy Mater. Sol. Cells.* 2011, **95**, 2516.

[46] D.B. Mi, J.B. Park, F. Xu, H.U. Kim, J.H. Kim, D.H. Hwang, *Bull. Korean Chem. Soc*. 2014, **35**, 1647.

[47] Y.M. Zhang, H. Tan, M.J. Xiao, X.C. Bao, Q. Tao, Y.F. Wang, Y. Liu, R.Q. Yang, W.G. Zhu, *Org. Electron*. 2014**, 15**, 1173.

Figures and Tables

Scheme 1. Molecular structure of TPA(DPP-PN)$_3$ and TPA-3DPP

Scheme 2. Synthetic route of TPA(DPP-PN)$_3$ and TPA-3DPP

Figure 1. TGA curves of TPA(DPP-PN)$_3$ and TPA-3DPP

Figure 2. Cyclic voltammograms of the TPA(DPP-PN)$_3$ and TPA-3DPP films on platinum electrode in acetonitrile solution containing 0.1 mol/L Bu_4NPF_6 at a scan rate of 100 mV s^{-1} by using ferrocene as an internal standard

Figure 3. UV-Vis absorption spectra of TPA-3DPP and TPA(DPP-PN)$_3$ in CH_2Cl_2 and in the neat films (a), as well as in their blend films with $PC_{71}BM$ at a optimized ratio of 1:2.5 (*w/w*) (b)

Figure 4. *J-V* characteristics of the OSCs with an active layer of TPA(DPP-PN)$_3$ (or TPA-3DPP) and $PC_{71}BM$ at a ratio of 1:2.5 (*w/w*) under illumination of AM1.5G, 100 mW cm^{-2}

Figure 5. External quantum efficiency curves of the optimized SMs/$PC_{71}BM$-based devices.

Figure 6. *J-V* characteristics of the hole-only TPA-3DPP and TPA(DPP-PN)$_3$ devices

Table 1. Electrochemical and thermal parameters for TPA(DPP-PN)$_3$ and TPA-3DPP.

Table 2. UV-Vis data of TPA(DPP-PN)$_3$, TPA-3DPP and their analogues in dichloro-methane solution ([c] = 10^{-5} mol L^{-1}) and in their neat films

Table 3. Photovoltaic parameters of the devices at a ratio of 1:2.5 (*w/w*) between TPA(DPP-PN)$_3$ (or TPA-3DPP or its analogues) and $PC_{71}BM$ under the illumination of AM 1.5 G solar irradiance(100 mW cm^{-2})

Table 1

Compounds	E_{ox}/V[a]	E_{red}/V[a]	E_{HOMO}/eV[b]	E_{LUMO}/eV[b]	E_g^{cv}/eV	T_d/ °C
TPA(DPP-P)$_3$	0.62	-0.89	-4.97	-3.46	1.51	386
TPA-3DPP	0.86	-0.99	-5.21	-3.36	1.85	409

[a] Onset oxidation and reduction potentials measured by cyclic voltammetry in solid films

[b] E_{HOMO} = [-(E_{ox}-0.45)-4.8] eV, E_{LUMO} = [-(E_{red}-0.45)-4.8] eV, where 0.45 V is the value for ferrocene vs. Ag/AgCl and 4.8 eV is the energy level of Ag/AgCl to the vacuum energy level.

Table 2

Compounds	$\lambda_{abs,sol}$/nm[a], ($\varepsilon \times 10^5/M^{-1}cm^{-1}$)	$\lambda_{max,film}$/nm	$\lambda_{onset,film}$/nm[b]	$E_{g,film}^{opt}$/ eV[c]	*ref*
TPA(DPP-PN)$_3$	632 (1.97)	673	776	1.60	this work
TPA-3DPP	593 (1.46)	622	679	1.83	this work
(P-DPP)$_3$TPA	623 (/)	645	720	1.72	42
(4-FP-DPP)$_3$TPA	623 (/)	647	730	1.70	42
(4-BuP-DPP)$_3$TPA	623 (/)	653	740	1.68	42

[a]In dilute dichloromethane solution. [b]Absorption edges of the films. [c]Optical bandgaps were determined using the equation $E_{g,\,film,}^{opt} = 1240/\lambda_{onset,\,film}$.

Table 3

Donor	Acceptor	D/A(w/w)	J_{sc}/ mA cm^{-2}	V_{oc}/ V	*FF*/ %	PCE_{max}/ %	*ref*
TPA(DPP-PN)$_3$	$PC_{71}BM$	1:2.5	8.95	0.80	51	3.67	this work
TPA-3DPP	$PC_{71}BM$	1:2.5	5.85	0.91	36	1.91	this work
TPA(DPP-PN)$_3$	$PC_{61}BM$	1:2.5	8.12	0.81	47	3.07	this work
(P-DPP)$_3$TPA	$PC_{61}BM$	1:3	8.53	0.78	32	2.13	42
(4-FP-DPP)$_3$TPA	$PC_{61}BM$	1:3	4.70	0.84	38	1.51	42
(4-BuP-DPP)$_3$TPA	$PC_{61}BM$	1:2	5.83	0.80	42	1.98	42

Scheme 1

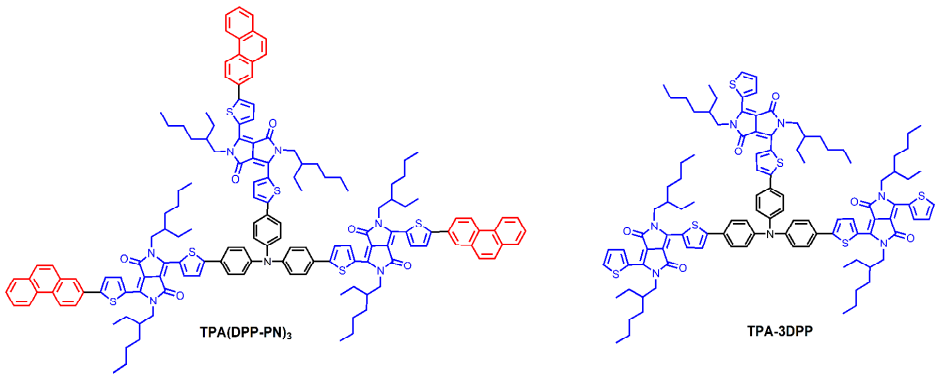

Scheme 2

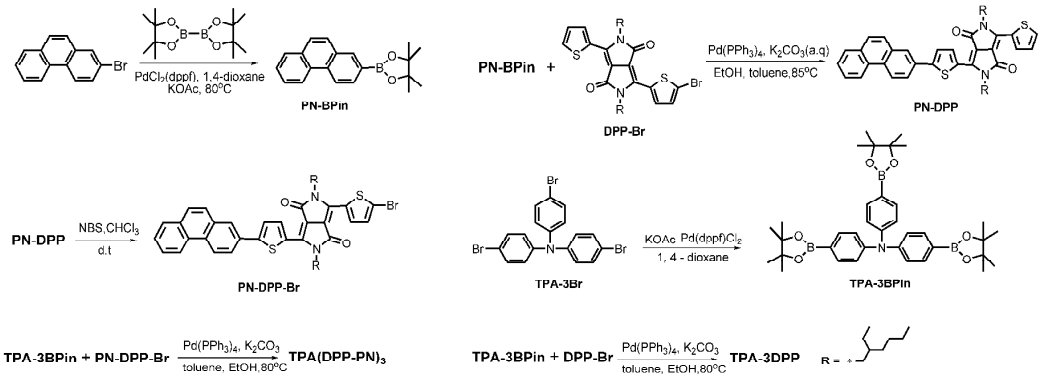

Figure 1

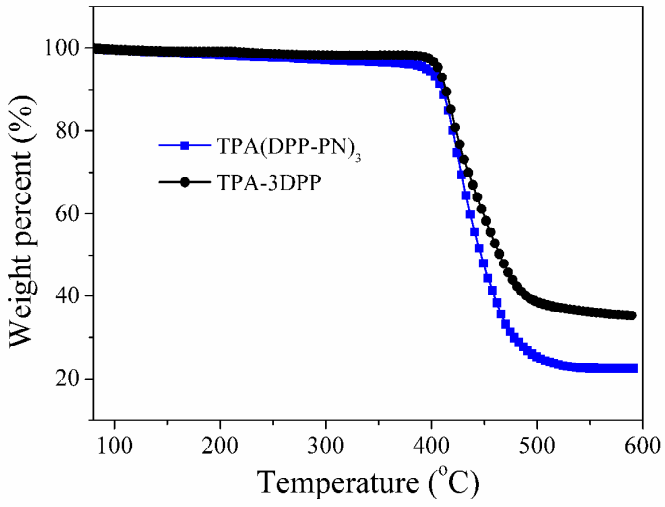

Figure 2

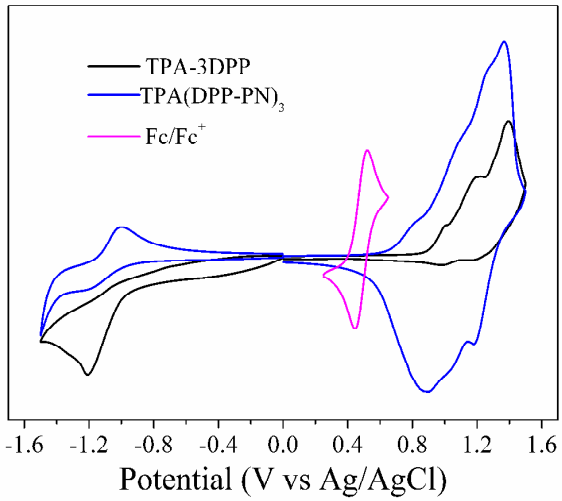

Figure 3a

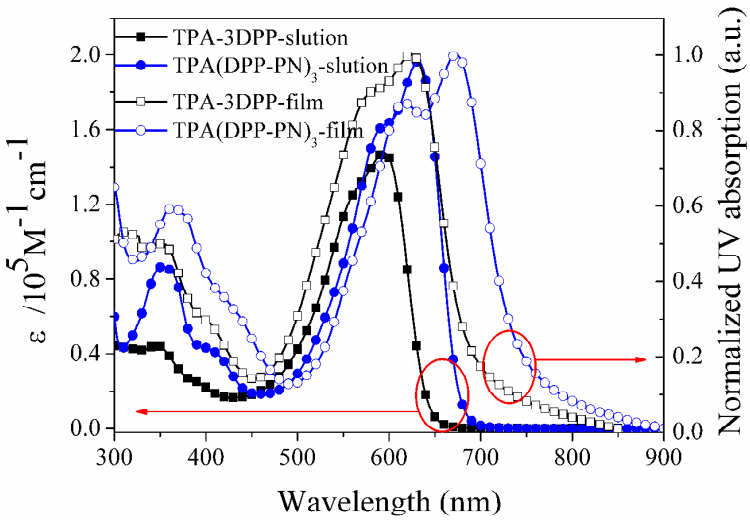

Figure 3b

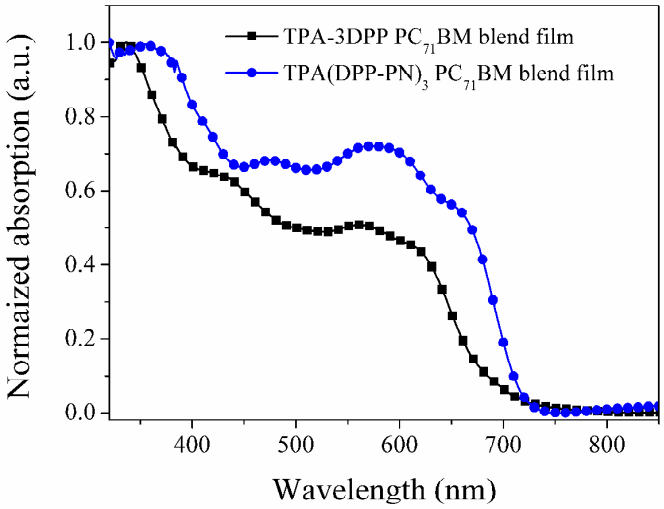

Figure 4

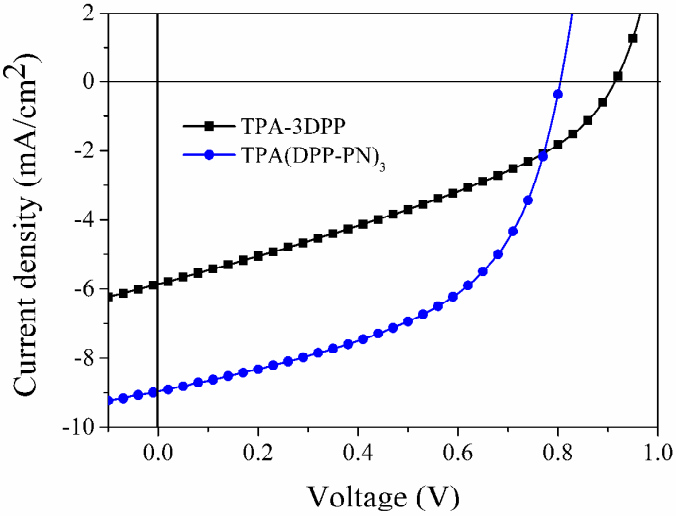

Figure 5

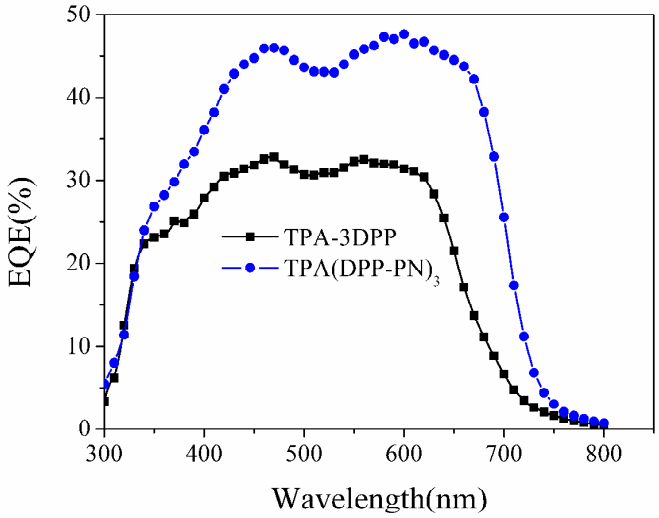

Figure 6

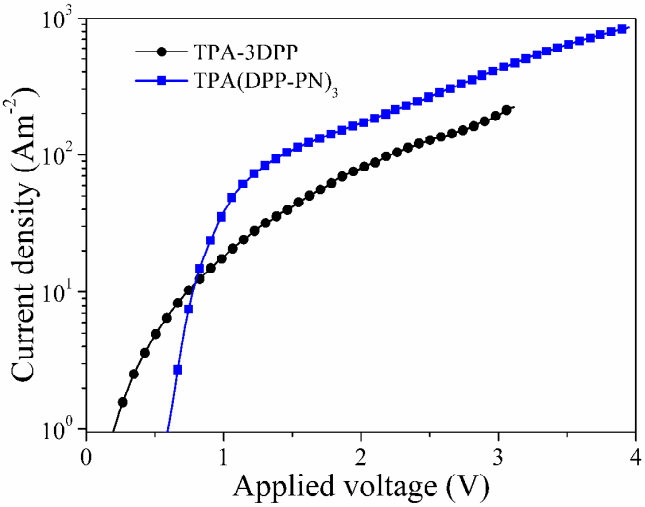

Graphical Abstract

Significantly improved photovoltaic performance of the triangular-spiral TPA(DPP-PN)$_3$ by appending planar phenanthrene units into the molecular terminals

Youming Zhang,[a] Xichang Bao,*[b] Manjun Xiao,[a,b] Hua Tan,*[a,c] Qiang Tao,[a] Yafei Wang,[a] Yu Liu,[a] Renqiang Yang*[b] and Weiguo Zhu*[a]

A new triangular-spiral small molecule of TPA(DPP-PN)$_3$ was obtained on the basis of the TPA-3DPP counterpart by pending planar phenanthrene units into the molecular terminals, which displayed an enhanced light-harvesting ability and improved hole mobility. Its organic solar cells further exhibited an improved photovoltaic performance with the best power conversion efficiency of 3.67% and a maximum short-circuit current density of 8.95 mA cm^{-2}, which are 1.9 and 1.5 times higher than those of the TPA-3DPP-based cells.